Solid-State NMR (^{19}F and ^{13}C) Study of Graphite Monofluoride $(CF)_n$: ^{19}F Spin−Lattice Magnetic Relaxation and ^{19}F/^{13}C Distance Determination by Hartmann−Hahn Cross Polarization

Jérôme Giraudet,[†,‡] Marc Dubois,[§] André Hamwi,[§] William E. E. Stone,[†] Pascal Pirotte,[†] and Francis Masin*[,†]

Matière Condensée et Résonance Magnétique, Université Libre de Bruxelles, CP 232, Boulevard du Triomphe, B-1050 Bruxelles, Belgium, and Laboratoire des Matériaux Inorganiques, UMR CNRS 6002-Université B. Pascal, 24 av. des Landais, 63177 Aubière Cedex, France

Received: July 16, 2004; In Final Form: October 21, 2004

Graphite monofluoride $(CF)_n$ was studied by solid-state NMR. ^{19}F spin−lattice relaxation time T_1 and second moment measurements of the ^{19}F line are presented. A "chair" conformation structure is found to be compatible with the experimental data. Relaxation is shown to be mainly due to paramagnetic oxygen. The presence of a molecular motion with an activation energy of 1.685 kJ·mol^{-1} (202.7 K) is also evidenced. ^{19}F magic angle spinning (MAS) NMR and ^{13}C MAS NMR with ^{19}F to ^{13}C cross-polarization allows the determination of CF and CF_2 groups. Reintroduction of dipolar coupling by cross-polarization is used for C−F bond length determination (0.138 ± 0.001 nm).

1. Introduction

Because of their numerous interesting properties, graphite fluoride and especially graphite monofluoride $(CF)_n$ have been the focus of a great number of studies. For example, graphite fluorides are used as solid lubricants[1,2] or cathode material in high energy density lithium batteries.[3,4] Graphite monofluoride was first synthesized in 1934 by Ruff et al.[5] who proposed a structure derived from graphite with C−F covalent bonds located both above and below every carbon atom of each graphene layer. In this case the hybridization of carbon is sp^3, leading to a loss of both aromatic character and flatness of the layers.

The structure of graphite monofluoride was initially shown to be formed either of an infinite array of trans-linked cyclohexane chairs ($a = b = 0.2553$ nm, $c = 0.5666$ nm, space group $P6_3mc$)[6,7] or an infinite array of cis−trans-linked cyclohexane boats ($a = 0.4511$ nm, $b = 0.2527$ nm, $c = 0.5673$ nm, space group $Pmm2$)[7,8] with an energy barrier for transition between chair and boat structures of 2.72 eV/unit cell.[7] Later, Touhara et al.[9] proposed a new model based on the chair structure with a mirror plane between the adjacent carbon layer planes ($a = b = 0.253-0.257$ nm; $c = 1.21$ nm; space group $P\bar{6}m2$. According to Charlier et al.,[7] Zajac et al.,[10] and Takagi et al.,[11] the theoretical C−F bond lengths are respectively 0.136−0.137 nm, 0.141−0.145 nm, and 0.135 nm. Experimentally Ebert et al.[8] estimated this C−F bond length to 0.140 nm. From neutron diffraction data, Sato et al.[12] determined this length to be 0.136 nm. The chair form is the most stable conformation. However, depending on the synthesis conditions, the amount of chair may vary as explained by Charlier et al.[7]

As shown by various authors, the type of conformation can be determined by NMR second moment measurements. Kita et al.[13] and Watanabe[14] both concluded that for their samples the chair conformation was dominant, on the contrary Ebert et al.[8] found that the boat type was favored. For the ^{19}F T_1 spin−lattice relaxation in $(C_2F)_n$, Panich et al.[15] mainly attributed it to the presence of localized paramagnetic centers. They found that, at 44 MHz, the T_1 value for $(CF)_n$, prepared from natural graphite, is longer (660 ms) than in $(C_2F)_n$ (53 ms). This difference was explained[15] by a larger number of paramagnetic centers in $(C_2F)_n$.

The aim of this paper is to contribute to a better understanding of the relaxation mechanisms in $(CF)_n$: presence of molecular motions and the effect of paramagnetic oxygen. Both ^{19}F NMR relaxation and electron paramagnetic resonance (EPR) measurements are used to this effect. ^{19}F and ^{19}F to ^{13}C cross-polarization (CP) experiments, under magic angle spinning (MAS), are also used in this work.

2. Experimental Section

2.1. Graphite Monofluoride Elaboration. The covalent graphite monofluoride was synthesized using the conventional method. A monel boat containing graphite is placed in a nickel reactor and heated to 600 °C under a pure F_2 gas flow. The formula of the obtained sample was checked to be $(CF)_n$.

2.2. Characterization. EPR spectra were run using an X band Bruker EMX spectrometer operating at 9.653 GHz at room temperature. Diphenylpicrylhydrazyl was used to calibrate the resonance frequency ($g \approx 2.0036 \pm 0.0002$) and densities of spins carriers. Data processing and simulations were performed using Bruker WIN-EPR and SimFonia software.

NMR experiments were performed on a Bruker MSL 300 spectrometer associated with a superconducting coil giving a magnetic field of 7.049 T (working frequency for ^{13}C and ^{19}F: 73.4 and 282.2 MHz, respectively). Measurements in the temperature range 4−470 K were obtained with an Oxford ITC4 controller. Two NMR Bruker probes were used: a static one and a special CP/MAS probe with fluorine decoupling on a

* Corresponding author: tel. +32 2 650 5755; fax + 32 2 650 5023; e-mail address fmasin@ulb.ac.be.
† Université Libre de Bruxelles.
‡ Present address: UMR CNRS 6002-Université B. Pascal.
§ UMR CNRS 6002-Université B. Pascal.

10.1021/jp046833j CCC: $30.25
Published on Web 12/04/2004

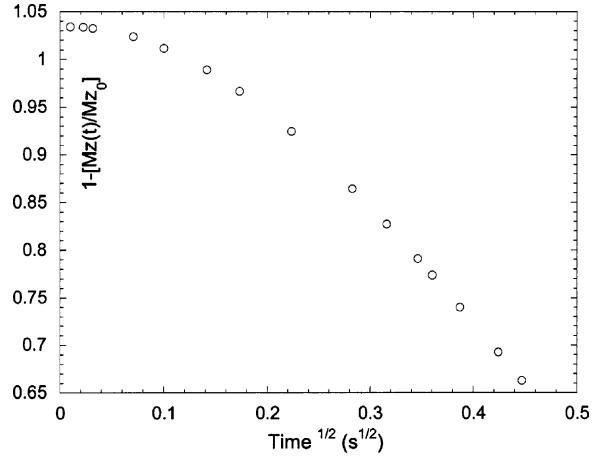

Figure 1. Initial ^{19}F magnetization curve of $(CF)_n$, $1 - M_z(t)/M_0$ versus $t^{1/2}$, in the presence of air and at room temperature.

4 mm rotor. The $^{19}F-^{13}C$ match was optimized on poly(tetrafluoroethylene) (PTFE) by adjustment of the ^{13}C power level to coincide with the previously determined ^{19}F $\pi/2$ pulse width. The spin−lattice relaxation time T_1 was measured using a saturation recovery sequence. The $\pi/2$ pulse width was between 1 and 5 μs. Second moments were determined via a solid echo sequence (two 4 μs $\pi/2$ pulses separated by 12 μs). ^{13}C and ^{19}F chemical shifts were externally referenced with respectively tetramethylsilane (TMS) and CF_3COOH. The chemical shift anisotropy (CSA) tensor was determined with the aid of the Bruker 1D WINNMR and WINMAS software. Low-frequency NMR ^{19}F experiments were recorded on a Maran Ultra spectrometer working at 18.9 MHz. In this case all experiments were carried out at 303 K.

3. Results and Discussion.

3.1. Second Moment M_2 and ^{19}F T_1 Spin−Lattice Relaxation. The second moments are directly determined from the ^{19}F NMR solid echo signal; they are then compared to theoretical values calculated with the Van Vleck formula.[16] For our $(CF)_n$ sample, the second moment is found to be 178.6×10^6 Hz^2 (11.1 G^2). According to Kita et al.,[13] the theoretical second moments for the chair and the boat structures are respectively 155.6×10^6 Hz^2 (9.7 G^2) and 348.2×10^6 Hz^2 (21.7 G^2). For the "mirror" structure proposed by Touhara et al.,[9] the calculated second moment is 165.0×10^6 Hz^2 (10.3 G^2). For our sample, just as for Kita et al.[13] and Watanabe[14] and contrary to Ebert et al.,[8] the chair structure is favored. A distinction between "normal" and "mirror" structure cannot be made by second moment measurements because of the small difference existing between theoretical values. When performed under normal air conditions, the measured ^{19}F spin−lattice relaxation times T_1 of our $(CF)_n$ are 450 and 260 ms, at 282.2 and 18.9 MHz, respectively. A similar result was found by Panich et al.[15] at 44 MHz and is attributed to the presence of paramagnetic centers. When this is the case and under certain conditions (when the spin diffusion constant is of an appropriate value), Blumberg[17] showed that the magnetization for short recovery times develops as $t^{1/2}$. As shown in Figure 1, for our samples the magnetization recovery is not at all linear in $t^{1/2}$.

This behavior, however, does not a priori exclude a relaxation mechanism governed by paramagnetic centers. In our sample, EPR shows (Figure 2) that the number of paramagnetic centers is low, 1.2×10^{19} spin·g^{-1} (1 for 1630 fluorine atoms).

The origin of the EPR lines is identified as carbon dangling bonds having a localized spin. Such spin carriers have been

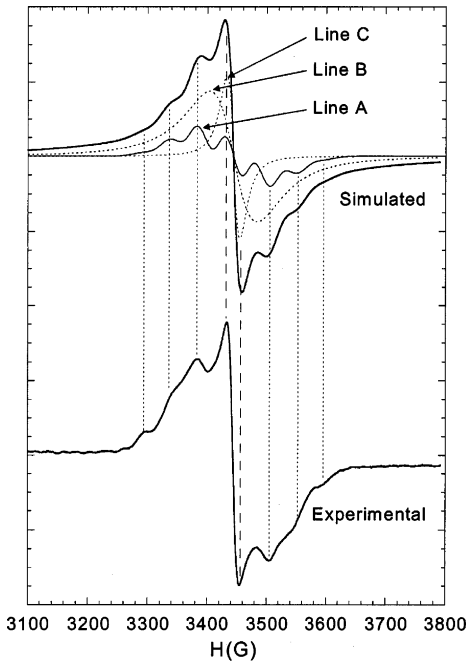

Figure 2. EPR spectra and simulation of $(CF)_n$.

proposed for other fluorinated carbons obtained in a F_2 atmosphere.[15,18,19] The g factor, which is typical for free radicals and localized structural defects, is close to 2.003 ± 0.002. A superhyperfine structure with seven lines is clearly observed (line denoted A, Figure 2). This phenomenon is due to the hyperfine interaction between dangling electron bonds and the six neighboring fluorine nuclei (nuclear spin $I = 1/2$), thus, yielding $2nI + 1 = 7$ lines. The simulation of the signal leads to a hyperfine parameter $A = 45 \pm 2$ G, a line width $\Delta H_{pp} = 36$ G ± 2 G, and a g factor of 2.003 ± 0.001. These EPR parameters are close to the ones proposed by Panich et al.[15] who have studied fluorinated petroleum cokes; in this study, the large line width is interpreted by the joint effect of dipole−dipole and exchange interactions between paramagnetic centers. Line B results from the unresolved hyperfine structure of the dangling electron bonds interacting with neighboring fluorine nuclei. Dangling bond centers could adopt with the surrounding fluorine atoms different configurations; this disorder then leads an unresolved hyperfine structure. An additional line is present in the EPR spectrum (denoted line C, $\Delta H_{pp} = 20 \pm 1$ G and $g = 2.003 \pm 0.002$) indicating that two types of dangling bonds (and/or defects with different environments) are present in the material.

To explain the origin of the short T_1 measured for our sample, we examined the effect of paramagnetic oxygen. It is observed that, when the sample is sealed under vacuum, the T_1 value of ^{19}F in $(CF)_n$ increases from 0.45 to 10.10 s while that of ^{13}C goes from 20.8 s to more than 400 s. This clearly shows that atmospheric oxygen constitutes an important source of relaxation for $(CF)_n$. Oxygen is probably localized between the grains of $(CF)_n$ or adsorbed on their surface. This influence of atmospheric oxygen on the T_1 values of $(CF)_n$, unreported until now, sheds some doubt about all previous conclusions published so far in the field. All the following results, therefore, relate solely to sealed samples. It is worth noting that, apart from eliminating oxygen, the effect of pumping does not modify the sample. Indeed, after being pumped, a sample which is replaced under normal atmospheric conditions recovers its original T_1 value.

Concerning the ^{19}F line width (full width at half-maximum, fwhm), it is observed that its temperature dependence (Figure

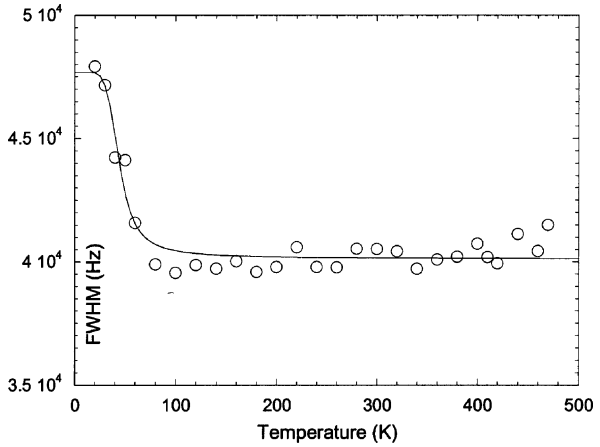

Figure 3. ^{19}F fwhm as a function of temperature. The solid line is a fit using eq 3. The value of the activation energy is extracted from the T_1 experiments.

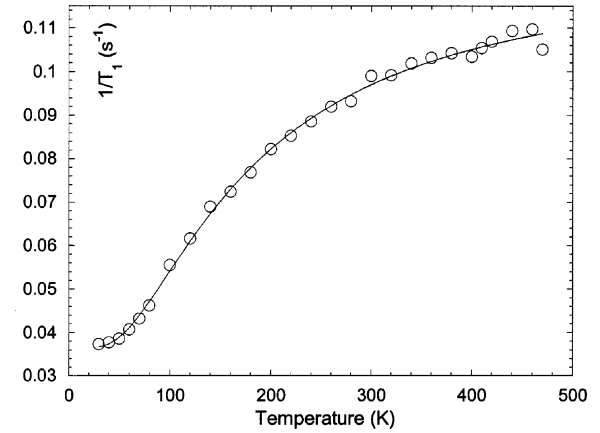

Figure 4. ^{19}F spin−lattice relaxation rate (s^{-1}) as a function of temperature (K). The solid line is a fit using the BPP model.

3) shows the well-known variation characteristic of dipole−dipole interactions.

The reduction of the fwhm (or second moment) at a high temperature results from molecular motional averaging. At a low temperature, the fwhm corresponds to "frozen" motionless molecules. The fwhm and second moment temperature reduction factors are 0.84 and 0.71, respectively. These values are small compared to the one found for solid benzene ($\approx$5)[20,21] and indicate the presence of a less efficient motion such as a small angular oscillation. The ^{19}F NMR spin lattice relaxation time T_1 of a vacuum-sealed $(CF)_n$ sample was measured between 4 and 470 K (Figure 4) at a frequency of 282.2 MHz. At each temperature, the recovery of magnetization is found to be a single exponential. For molecular motions, the theory of Bloembergen, Purcell, and Pound (BPP)[22] allows us to write the following expression for the T_1 temperature dependence:

$$\frac{1}{T_1} = A\left[\frac{\tau}{1+\omega^2\tau^2} + \frac{4\tau}{1+4\omega^2\tau^2}\right] \qquad (1)$$

where A is proportional to $\gamma^2 h_0^2$, γ is the magnetogyric constant of fluorine ($25.162\,333 \times 10^7$ rad·s^{-1}·T^{-1}), h_0 is the amplitude of the fluctuating magnetic field, ω is the nuclear spin resonance frequency ($\omega = 2\pi\nu$ and $\nu = 282.2$ MHz for fluorine), and τ is the correlation time. The process is thermally activated and described by an Arrhenius law:

$$\tau = \tau_0 e^{E/T} \qquad (2)$$

where E is the activation energy.

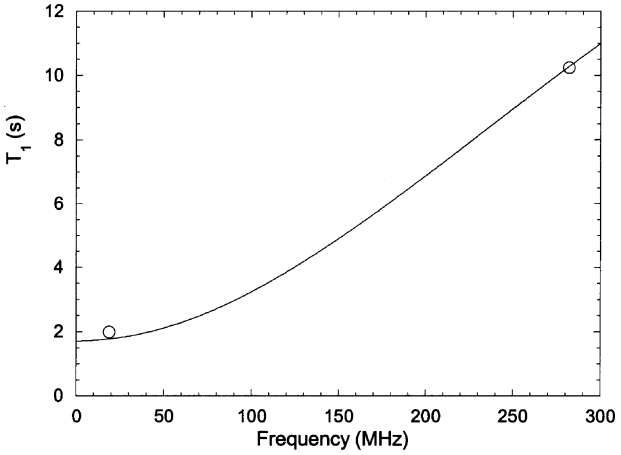

Figure 5. Spin−lattice relaxation time (T_1) as function of frequency. The full line represents the calculated data with the fit parameters of Table 1. The two circles represent the experimental data at 18.9 and 282.2 MHz. All T_1 were measured at 303 K in the absence of oxygen.

TABLE 1: Parameters Obtained by Fitting the ^{19}F $1/T_1$ Data

parameter	value	error
A (Hz^2)	1.2879×10^8	1.81×10^7
τ_0 (s)	6.0841×10^{-10}	1.33×10^{-10}
E (T)	202.7	13.79
E (kJ·mol^{-1})	1.685	0.1147
E (meV)	17.46	1.188

The T_1 curve can be fitted using eqs 1 and 2 (see Figure 4 and corresponding parameters in Table 1). The extracted activation energy ($E = 1.685$ kJ·mol^{-1} or 202.7 K) is too small to attribute the motion to an exchange between the chair and the boat conformations. More probably, this energy represents a C−F bond motion. For comparison in benzene[23] the activation energy of rotation around an axis perpendicular to the molecule is 16.8 kJ·mol^{-1}.

Expression 1 also contains a frequency parameter which can be used (in this case the temperature is kept constant). T_1 variations as a function of frequency (Figure 5) can be calculated with expression 1 using the fit parameters of Table 1. A value of T_1 has been measured at 303 K at a frequency of 18.9 MHz (in the absence of oxygen) and compared to the estimated value (Figure 5). The experimental $T_1 = 1.99$ s is found to be in good agreement with the calculated value, thus, confirming the hypothesis that molecular motion may be responsible for the observed spin lattice relaxation. T_1 has been also been measured at this frequency in the presence of air; T_1 is equal to 0.26 s instead of 0.45 s at 282.2 MHz, so the value at 44 MHz could be estimated near 0.3 s. So, at this frequency, T_1 of our sample differs only by a factor 2 from the T_1 reported in ref 15 for similar $(CF)_n$. This difference can be explained by different amounts of adsorbed oxygen on the two samples due to the diversity of the grain surfaces.

This can be reinforced by fitting the fwhm data by the expression[22]

$$\text{fwhm} = A + \frac{2B}{\pi}\arctan\left[C\exp\left(\frac{E}{T}\right)\right] \qquad (3)$$

where A is the line width at high temperature, B is the contribution to the line broadening from the relaxation mechanism, C is a constant, and E is the activation energy. Using the activation energy determined above from the ^{19}F relaxation, parameters A, B, and C can be deduced (Table 2). The fwhm experimental data can be nicely fitted by using just one

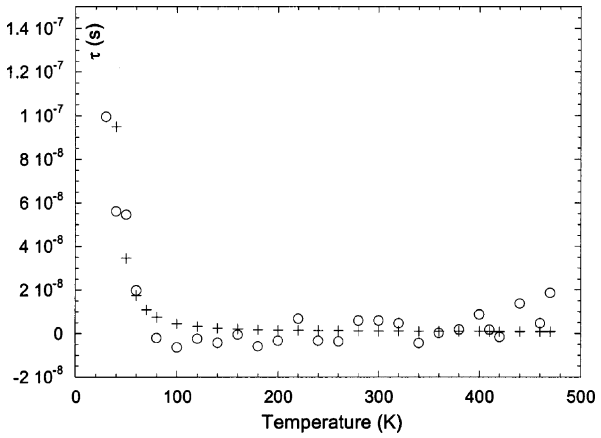

Figure 6. Correlation time as function of temperature. Experimental data are represented by circles ($\alpha = 1$, $L = 409 \times 10^6$ Hz^2, and $l = 288 \times 10^6$ Hz^2). Crosses represent the values calculated from the Arrhenius law ($\tau_0 = 6.0841 \times 10^{-10}$ s and $E = 1.685$ kJ·mol^{-1}).

TABLE 2: Parameters Obtained by Fitting the fwhm Data with Expression 3

parameter	value	error
A (Hz)	40 058	151.0
B (Hz)	7644	438.0
C (Hz)	0.0109	0.0024

activation energy. Molecular motion is progressively slowed until frozen at around 80 K, which corresponds to a motional frequency of 7644 Hz.

An experimental correlation time $\tau(T)$ for each temperature can be extracted from the second moment value $M_2(T)$ by relation 4:[24]

$$\tau(T) = \frac{1}{\alpha 4\pi M_2(T)} \tan\left[\frac{\pi}{2}\frac{M_2^2(T) - l^2}{L^2 - l^2}\right] \qquad (4)$$

where α is a form factor near 1, L is the second moment of the rigid structure, and l is its reduced high-temperature value. Experimental τ values obtained from relation 4 (with the values of L and l determined from Figure 3) are given in Figure 6 together with the theoretical τ values calculated from the temperature-activated T_1 fit. A good agreement between experimental and theoretical τ values is clearly seen.

Whereas the spin−lattice relaxation time T_1 is characteristic of relaxation mechanisms occurring at frequencies close to the Larmor frequency (in this case, 282.2 MHz), the dipolar relaxation time T_{1d} is sensitive to mechanisms occurring at frequencies approaching 0. T_{1d} is measured by the so-called Jeener−Broekaert sequence.[25] Figure 7 shows the evolution of T_{1d} as a function of temperature together with certain magnetization curves at a given temperature. Relaxation times are extracted from the magnetization curves by using relation 5:

$$M(\tau) = M_0 e^{-\tau/T_{1d}} \qquad (5)$$

Practically no temperature dependence for T_{1d} is found, which implies that the corresponding relaxation mechanisms at low frequencies are also temperature-independent.

3.2. ^{19}F MAS and ^{13}C CP MAS Studies. Figure 8a shows a ^{19}F MAS NMR spectrum of $(CF)_n$ obtained at a spinning rate of 15 kHz. Two isotropic lines are present. In agreement with the work of Krawietz and Haw,[26] the most intense line at −102 ppm is attributed to C−F groups while the second line at −31 ppm is either assigned to CF_2 groups located at the edge of

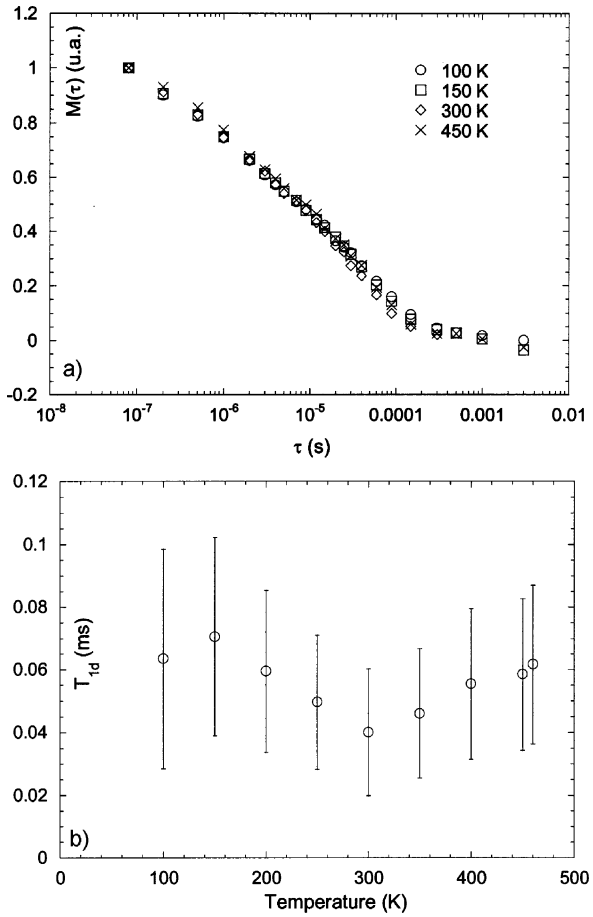

Figure 7. (a) ^{19}F magnetization after a Jeener−Broekaert sequence at 100, 150, 300, and 450 K. (b) Dipolar relaxation time T_{1d} as a function of temperature.

graphite layers or associated with structural defects. Spinning sidebands are also present for each line.

A ^{19}F to ^{13}C CP MAS spectrum at 15 kHz is shown in Figure 8b-1. Two lines corresponding to CF and CF_2 groups are found at 88 and 111 ppm, respectively. These attributes are in agreement with previous results[26−29] carried out on fluorinated carbons. The line surface ratio of the CF and CF_2 groups could in principle be used to determine the size of the graphitic layers. However, this is not possible because CP results are not quantitative. ^{13}C lines recorded without CP (not shown here) show very poor resolution with no distinct CF_2 line. When run under static conditions (i.e., no MAS; Figure 8b-3), only one non-Gaussian line is present at 100 ppm. The line shape in this case is governed by CSA; its isotropic value can be extracted from the MAS high-rotation spectra (line at 88 ppm). The CSA tensor can be calculated using the Herzfeld and Berger method[30] based on the presence of some sidebands within the line width. A sufficient number of well-separated sidebands can be obtained at 2 kHz (Figure 8b-2 and Table 3 for the values obtained).

The C−F bond length which is included in the expression of the dipolar interaction D_{IS} is an important information which can also be determined by NMR. Several techniques such as rotational echo double resonance[31] (REDOR) and transferred echo double resonance[32,33] (TEDOR) have been developed for the study of dipolar interactions. In this study, the dipolar couplings are reintroduced into the spectrum by using Hartmann−Hahn CP associated to MAS. For static samples, the Hartmann−Hahn matching conditions correspond to $\omega_{1I} = \omega_{1S}$ where ω_{1I} and ω_{1S} are the amplitudes of the radio frequency fields applied respectively to the abundant spins I having a high

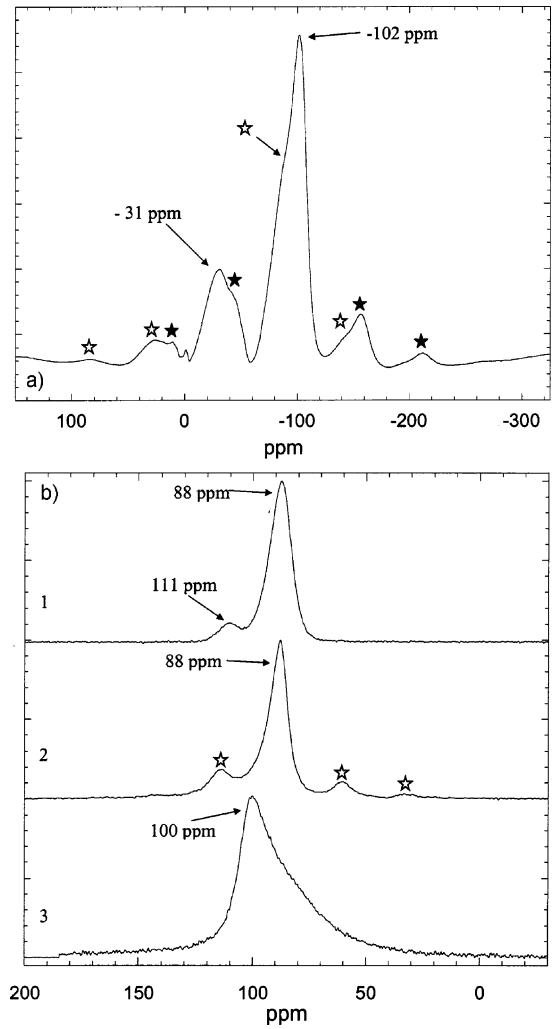

Figure 8. (a) ^{19}F MAS NMR spectrum of graphite monofluoride at a speed of 15 kHz. White and black stars denote spinning sidebands at −31 and −102 ppm. (b) ^{13}C MAS NMR spectra of graphite monofluoride obtained with ^{19}F to ^{13}C CP. Spectra at spinning speeds of 15 (1) and 2 kHz (2) and static (3). Stars denote spinning sidebands.

TABLE 3: Experimental Values of the CSA Tensor Determined by the Herzfeld and Berger Method[30]

d_{iso} (ppm)	d_{11} (ppm)	d_{22} (ppm)	d_{33} (ppm)
88.3	111.4	105.1	48.5

gyromagnetic ratio and to the rare spins S with low gyromagnetic ratio.[34] When the samples are rotated and the spinning frequency (ω_r) exceeds both the I−I and the S−S dipolar interactions, then the Hartmann−Hahn condition is split into a series of new sidebands with $\Delta = \omega_{1I} - \omega_{1S} = n\omega_r$, where n is the sideband matching condition. It is well know that efficient CP can be obtained for $n = \pm 1, \pm 2$.[35,36] In this case, the amplitude of the CP signal at short contact times is found to be oscillatory with a frequency linked to the C−F bond length.[37] For spinning samples, the transferred polarization $M_s(t)$ evolves as

$$M_s(t) = \frac{\gamma_I}{\gamma_S} M_{0S} * \left[1 - \frac{1}{m+1}\exp\left(-\frac{t}{\tau_d}\right) - \frac{m}{m+1}\exp\left(-\frac{t}{2\tau_c}\right)\cos(2\pi\varphi t)\right] \quad (6)$$

where τ_d is the characteristic diffusional time of interaction between the SI_m group and the spin reservoir; τ_c is the correlation time of the dipolar fluctuation and a good estimate for τ_c is given by the abundant spins second moment M_2^{II} as $\tau_c = [8/(5M_2^{II})]^{1/3}$; m is the number of fluorine atoms per carbon which are involved in the dipolar interaction; and $\varphi_{\pm n}$ is the angular dependence of the dipolar interaction

$$\varphi_{\pm 1} = \frac{D_{IS}}{4}\sqrt{2}\sin 2\beta \quad (7)$$

$$\varphi_{\pm 2} = \frac{D_{IS}}{4}\sin^2\beta \quad (8)$$

$$D_{IS} = \frac{\mu_0 \gamma_I \gamma_S \hbar}{4\pi r^3} \quad (9)$$

where β is the angle between the SI direction and the rotor axis. In practice, an inverse CP sequence is used with (i) the offsets of ^{19}F and ^{13}C exactly on resonance and (ii) the Hartmann−Hahn condition matched with $n = +1$. The CP dynamics is obtained by measuring the integrated peak intensity of the carbon spectra as a function of contact time. According to Bertani et al.,[37] in our case, for $n = +1$, the value of β is $\pi/4$ and the heteronuclear interaction is written as

$$\varphi_{\pm 1} = \frac{D_{IS}}{2\sqrt{2}} \quad (10)$$

The C−F bond length is then determined by relation 11, which is easily obtained from relations 9 and 10.

$$r_{CF} = \sqrt[3]{\frac{10\,046.3}{\varphi}} \quad \text{(nm)} \quad (11)$$

Figure 9a illustrates the evolution of the ^{13}C magnetization of the C−F group at a spinning rate of 15 kHz. As expected, an oscillatory behavior in the signal amplitude is observed. The rapid attenuation of the oscillation is due to a short $T_{1\rho}$ relaxation time. τ_d, τ_c, and φ are obtained by fitting the experimental data, and the results are summarized in Table 4.

From eq 11, the extracted φ value of 3729.3 Hz leads to a C−F bond length of 0.139(1) nm.

Distance determinations can also be deduced from the Fourier transform (Pake-like structure) of the ^{13}C magnetization evolution. The line splitting S1 between the intense singularities of the Pake pattern is used as a measure of the heteronuclear interaction with $D_{IS} = (2)^{1/2}S1$.[37] The obtained spectrum (Figure 9b) gives us a value of 7720 Hz for S1, and by consequence a distance equal to 0.137(6) nm is obtained from relation 12:

$$r_{CF} = \sqrt[3]{\frac{20\,092.6}{S1}} \quad \text{(nm)} \quad (12)$$

Contrary to the distance obtained by the fitting procedure, this value is model-free. The central peak at 0 Hz is a Fourier transform calculation artifact due to the nonoscillating term of eq 6 plus the fact that the magnetization does not go to 0 for long contact times. An indication of the precision of our measurement is given by the difference between the two values. Our average NMR value for the C−F bond, 0.138 ± 0.001 nm, is larger than the theoretical ones determined by Charlier et al.[7] (0.136−0.137 nm) and Takagi et al.[11] (0.135 nm) in their respective studies and than the experimental value of Sato et al.[12] (0.136 nm); it is, however, smaller than the values proposed by Zajac et al.[10] (0.141−0.145 nm) and Ebert et al.[8] (0.140 nm).

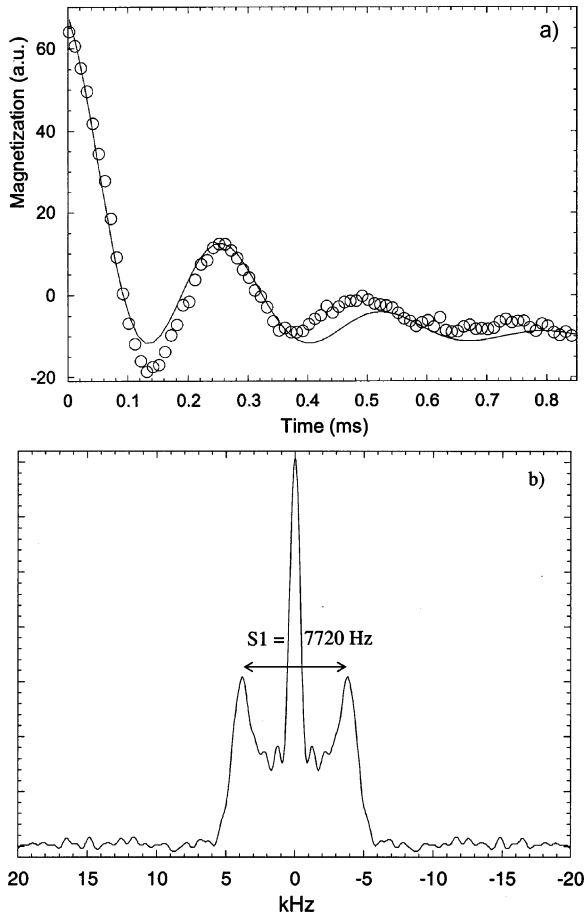

Figure 9. (a) Time evolution of the ^{13}C magnetization for the C−F group with a spinning speed of 15 kHz at the $n = +1$ Hartmann−Hahn condition. (b) Fourier transform of part a.

TABLE 4: Parameters Obtained by Fitting the ^{13}C Magnetization Evolution

τ_d (s)	τ_c (s)	φ (Hz)
$0.134\,24 \times 10^{-3} \pm 8.912 \times 10^{-6}$	$0.111\,12 \times 10^{-3} \pm 5.429 \times 10^{-6}$	3729.3 ± 32

Our C−F bond length is in fact overestimated by the presence of the motion discussed above. Indeed as the second moment (inversely proportional to the distance C−F) is reduced by molecular motions, the distance seen by NMR increases. We can take this fact into account by defining the ratio d_{th-exp}/d_{NMR}, where d_{th-exp} and d_{NMR} are respectively theoretical (or experimental) and NMR C−F bond lengths. A heteronuclear second moment reduction factor is then defined by $M_2^{IS}{}_{Motion}/M_2^{IS}{}_{Static} = (d_{th-exp}/d_{NMR})^6$. To try to explain which kind of motion could be responsible for the observed C−F bond length overestimation, we used the motional model described in Figure 10 where δ is the angle of oscillation from the equilibrium position and θ is the angle with respect to the rotation axis. The reduction factor is then easily calculated from

$$\frac{M_2^{IS}{}_{Motion}}{M_2^{IS}{}_{Static}} = 1 - 3\sin^2\theta\left[1 - \left(\frac{\sin\delta}{\delta}\right)^2\right] + \frac{9}{4}\sin^4\theta\left[1 - \frac{4}{3}\left(\frac{\sin\delta}{\delta}\right)^2 + \frac{1}{3}\left(\frac{\sin 2\delta}{2\delta}\right)^2\right] \quad (13)$$

Table 5 summarizes the C−F bond lengths given in the literature[7,11,12] together with the reduction factor, obtained from our experimental value, and corresponding δ. As shown by the use of this simple crude model, the relaxation mechanism (in an oxygen-free atmosphere) can indeed be explained as by a simple molecular motion. Of course this model is only a tentative proposal to explain the overestimation of the C−F bond length; on no account do we think that it is the only motion possible.

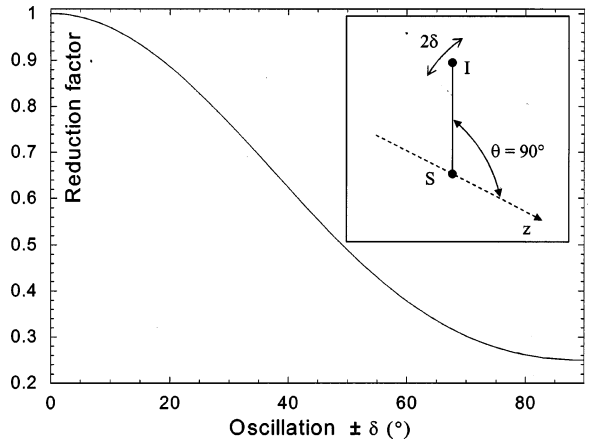

Figure 10. Angular dependence of the heteronuclear second moment reduction, determined from the model schematized in the inset with $\theta = 90°$.

TABLE 5: Heteronuclear Second Moment Reduction Factor and δ Data for the C−F Bond Length[a]

	d_{th-exp} (nm)	reduction factor	δ (deg)
theoretical	0.136−0.137[7]	0.916−0.957	17−12
	0.135[11]	0.876	21
experimental	0.136[12]	0.916	17

[a] Determined from Figure 10. The experimental NMR C−F bond length is $d_{NMR} = 0.138$ nm. The reduction factor is written $M_2^{IS}{}_{Motion}/M_2^{IS}{}_{Static} = (d_{th-exp}/d_{NMR})^6$.

4. Conclusion

In this study, an analysis of the ^{19}F spin−lattice relaxation time of graphite monofluoride $(CF)_n$ has shown that the presence of atmospheric paramagnetic oxygen is paramount in relaxing the nuclei. On the other hand, paramagnetic centers present within the sample are not the main cause of relaxation. The presence of a molecular motion with an activation energy of 1.685 kJ mol^{-1} has been found. ^{19}F MAS and ^{13}C MAS obtained with CP show the presence of CF and CF_2 groups. By reintroducing the dipolar coupling through CP techniques, a C−F bond length as seen by NMR (0.138 nm) has been determined. This value, which is the apparent NMR value, is compared to theoretical or experimental values determined elsewhere by using a simple model of oscillation of the C−F bond.

Acknowledgment. J.G. acknowledges financial help from the Région Auvergne (France). The authors would like to thank the BNB and FNRS (Belgium) for financial support.

References and Notes

(1) Fusaro, R. L.; Sliney, H. E. *ASLE Trans.* **1970**, *1* (1), 56−75.
(2) Fusaro, R. L. *Wear* **1979**, *53* (2), 303−315.
(3) Watanabe, N.; Endo, M.; Ueno, K. *Solid State Ionics* **1980**, *1* (5−6), 501−507.
(4) Touhara, H.; Fujimoto, H.; Watanabe, N.; Tressaud, A. *Solid State Ionics* **1984**, *14* (2), 163−170.
(5) Ruff, O.; Bretschneider, O.; Ebert, F. *Z. Anorg. Allg. Chem.* **1934**, *217*, 1−19.

(6) Rudorff, W.; Rudorff, G. *Z. Anorg. Allg. Chem.* **1947**, *253*, 281−296.
(7) Charlier, J. C.; Gonze, X.; Michenaud, J. P. *Phys. Rev. B* **1993**, *47* (24), 16162−16168.
(8) Ebert, L. B.; Brauman, J. I.; Huggins, R. A. *J. Am. Chem. Soc.* **1974**, *96* (25), 7841−7842.
(9) Touhara, H.; Kadono, K.; Fujii, Y.; Watanabe, N. *Z. Anorg. Allg. Chem.* **1987**, *544*, 7−20.
(10) Zajac, A.; Pelikan, P.; Minar, J.; Noga, J.; Straka, M.; Banacy, P.; Biskupic, S. *J. Solid State Chem.* **2000**, *150* (2), 286−293.
(11) Takagi, Y.; Kusakabe, K. *Phys. Rev. B* **2002**, *65* (12), 121103/1−121103/4.
(12) Sato, Y.; Itoh, K.; Hagiwara, R.; Fukunaga, T.; Ito, Y. *Carbon* **2004**, *42* (14), 2897−2903.
(13) Kita, Y.; Watanabe, N.; Fujii, Y. *J. Am. Chem. Soc.* **1979**, *101* (14), 3832−3841.
(14) Watanabe, N. *Physica B* **1981**, *105* (1−3), 17−21.
(15) Panich, A. M.; Shames, A. I.; Nakajima, T. *J. Phys. Chem. Solids* **2001**, *62* (5), 959−964.
(16) Van Vleck, J. H. *Phys. Rev.* **1948**, *74* (9), 1168−1143.
(17) Blumberg, W. E. *Phys. Rev.* **1960**, *119*, 79−84.
(18) Yokomichi, H.; Hayashi, T.; Amano, T.; Masuda, A. *J. Non-Cryst. Solids* **1998**, *227*−*230*, 641−644.
(19) Davidov, R.; Milo, O.; Palchan, I.; Selig, H. *Synth. Met.* **1983**, *8* (1−2), 83−87.
(20) Andrew, E. R. *J. Chem. Phys.* **1950**, *18*, 607−618.
(21) Andrew, E. R.; Eades, R. G. *Proc. R. Soc. London, Ser. A* **1953**, *218*, 537−552.
(22) Bloembergen, N.; Purcell, E. M.; Pound, R. V. *Phys. Rev.* **1948**, *73*, 679−712.
(23) Van Steenwinkel, R. *Z. Naturforsch., A: Phys. Sci.* **1969**, *24* (10), 1526−1531.
(24) Gutowsky, H. S.; Pake, G. E. *J. Chem. Phys.* **1950**, *18* (2), 162−170.
(25) Jeener, J.; Broekaert, P. *Phys. Rev.* **1967**, *157* (2), 232−240.
(26) Krawietz, T. R.; Haw, J. F. *Chem. Commun.* **1998**, *19*, 2151−2152.
(27) Mallouk, T.; Hawkins, B. L.; Conrad, M. P.; Zilm, K.; Maciel, G. E.; Bartlett, N. *Philos. Trans. R. Soc. London, Ser. A* **1985**, *314*, 179−183.
(28) Hagaman, E. W.; Murray, D. K.; Cul, G. D. D. *Energy Fuels* **1998**, *12* (2), 399−408.
(29) Panich, A. M. *Synth. Met.* **1999**, *100* (2), 169−185.
(30) Herzfeld, J.; Berger, A. E. *J. Chem. Phys.* **1980**, *73* (12), 6021−6030.
(31) Gullion, T.; Schaefer, J. *J. Magn. Reson.* **1989**, *81* (1), 196−200.
(32) Hing, A. W.; Vega, S.; Schaefer, J. *J. Magn. Reson.* **1992**, *96* (1), 205−209.
(33) Hing, A. W.; Vega, S.; Schaefer, J. *J. Magn. Reson., Ser. A* **1993**, *103* (2), 151−162.
(34) Hartmann, S. R.; Hahn, E. L. *Phys. Rev.* **1962**, *128*, 2042−2053.
(35) Stejskal, E. O.; Schaefer, J.; Waugh, J. S. *J. Magn. Reson.* **1977**, *28* (1), 105−112.
(36) Meier, B. H. *Chem. Phys. Lett.* **1992**, *188* (3−4), 201−207.
(37) Bertani, P.; Raya, J.; Reinheimer, P.; Gougeon, R.; Delmotte, L.; Hirschinger, J. *Solid State Nucl. Magn. Res.* **1999**, *13*, 219−229.